ACS APPLIED MATERIALS & INTERFACES

Research Article

www.acsami.org

# Facile Fabrication of Graphene Membranes with Readily Tunable Structures

Ge Shi,[†] Qingshi Meng,[†] Zhiheng Zhao,[†] Hsu-Chiang Kuan,[‡] Andrew Michelmore,[§] and Jun Ma*[,†]

[†]School of Engineering and [§]Mawson Institute, University of South Australia, Adelaide, South Australia SA5095, Australia

[‡]Department of Energy Application Engineering, Far East University, Tainan County 744, Tainan City, Taiwan

Supporting Information

**ABSTRACT:** Advanced membranes that combine mechanical robustness with fast permeation are crucial to many applications such as water purification, ions selectivity, and gas separation. Graphene sheets offer a promising opportunity to fabricate thin, high-flux, and pressure-endurable membranes because of their unique 2D morphology, oxidizable surface, and electrical conductivity. We herein report a highly effective yet simple approach to the fabrication of graphene membranes featuring controllable oxidation degrees and thus tunable structures and properties. The graphene sheets comprise a single or a few layers with a lateral dimension of 50−100 nm; their C/O ratios can be manipulated from 4.1 for graphene with a low degree of oxidation (low-oxidation graphene) to 2.5 for medium-oxidation graphene to 1.3 for high-oxidation graphene, by controlling the proportion of phosphoric acid during the 60 min fabrication. Fabricated by simple vacuum filtration, the membranes exhibited various water flux from 200.0 to 20.0 L/m$^2$·h·bar at 3 bar of pressure and mechanical robustness (Young's modulus can be up to 20 GPa and tensile strength to 100 MPa). When these membranes were used as electrodes for supercapacitors, specific capacitances of 58.8 F/g and 23.5 F/cm$^3$ were recorded for the low-oxidation graphene membrane at 1 A/g by a two-electrode configuration; the capacity values retained ~95% after 800 cycles; the high capacitance would be caused by moderate wettability and high electrical conductivity.

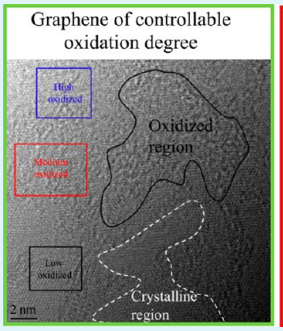


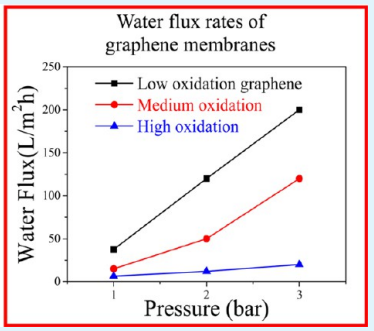


**KEYWORDS:** *graphene membranes, composites, graphene oxide, water permeation and specific capacitance*

## 1. INTRODUCTION

Laminar graphene oxide (GO) membranes have recently been developed by assembling through the vacuum filtration of micrometer-sized GO sheets, and they exhibit impressive performances including intensive hydrophilism, outstanding mechanical strength, and good flexibility.[1,2] Specifically, these membranes are formed by the self-alignment of GO sheets based on several mechanisms, including gravitational force, steric hindrance, and "excluded volume" interactions between GO sheets having large lateral dimensions.[3] Because pristine graphene is hydrophobic and cannot be processed in solution, GO has been developed by heavily oxidizing graphite, such as the methods proposed by Brodie,[4] Hummers and Offeman,[5] and recently Tour et al.[6] The presence of oxygen functional groups on both the basal planes and edges of individual GO sheets enables GO membranes to be further modified or intercalated by ions,[7] carbon nanotubes,[8] or organics,[9] and thereby the membranes can possess enhanced mechanical, conductive, and supercapactive properties. These membranes have extensive applications, such as transparent conductors,[10] electrodes for supercapacitors,[11] and matrices for water filtration.[12]

However, GO membranes lack a high filtration rate for fast water permeation[2,13] because the oxidization often creates too many hydrophilic groups, firmly locking water molecules. In addition, GO is limited by many irreversible defects and disorders.[14] Although subsequent reduction could remove all surface functional groups, taking carbon atoms in the form of CO and $CO_2$, posing add-on costs, the defects cannot get fixed completely while additional new defects were created,[15−18] which sacrifice the mechanical properties of the membrane. It is worth noting that desired C/O ratios 1.6−8.9 may be achieved by manipulating the reduction temperature or chemicals,[19−26] but the cost might pose a barrier to massive production. Therefore, it is of significance to develop an efficient, simple method to fabricate graphene membranes featuring controllable oxidation degrees and thus tunable structures and properties; any forms of harsh oxidation or reduction should be eliminated for cost-effectiveness. A critical step is to fabricate graphene sheets with a desired degree of oxidation.

We in this study report the development of free-standing graphene membranes through simple vacuum filtration of the stable aqueous suspension of graphene sheets; the sheets with readily controllable oxidation degrees are fabricated by

Received: January 6, 2015
Accepted: June 1, 2015
Published: June 1, 2015





DOI: 10.1021/am5091287
ACS Appl. Mater. Interfaces 2015, 7, 13745−13757

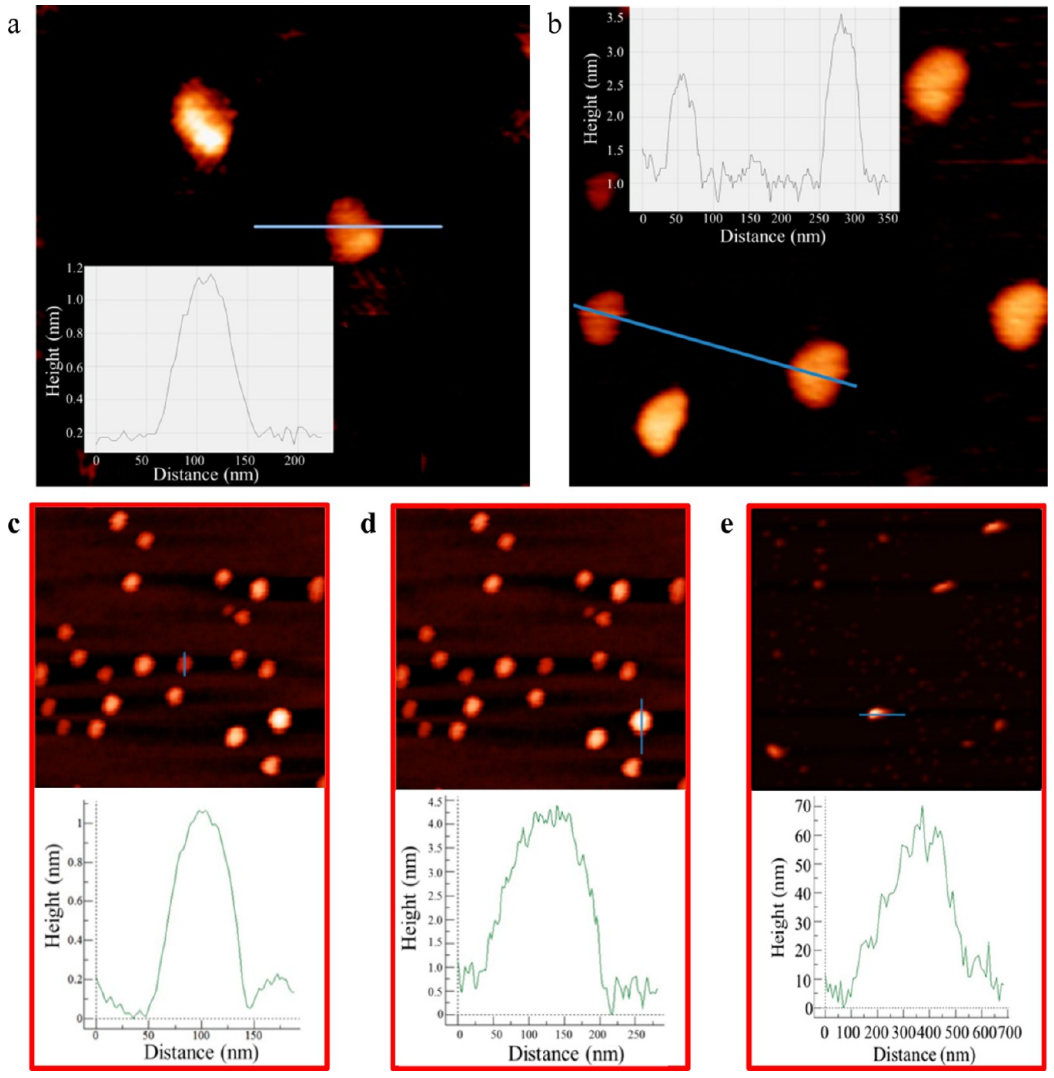


**Figure 1.** AFM images of graphene sheets with a high degree of oxidation: (a and b) at high magnification and 1−3 nm thickness; (c and d) at low magnification and ∼100 nm lateral dimension. Image and height profile of raw graphite particles (e) with ∼70 nm thickness and 600 nm lateral dimension.

simultaneously oxidizing and ultrasonicating graphite within 1 h, where phosphoric acid is employed as the buffer solvent to adjust the oxidization degree. The membranes also show competitive performance as the electrode material for supercapacitors.

## 2. EXPERIMENTAL SECTION

**2.1. Materials.** Graphite powder (Micro 0850) was provided by Asbury Carbons Pty Ltd. Potassium permanganate, sulfuric acid (95−98 wt %), and phosphoric acid (85 wt %) were purchased from Sigma-Aldrich. Hydrogen peroxide (30 wt %) was bought from Chem-Supply.

**2.2. Fabrication of Oxidation Graphene Sheets.** Graphene sheets with a low degree of oxidation (low-oxidation graphene) were prepared as below. $KMnO_4$ (0.4 g) was dissolved in a mixture of $H_2SO_4$ (13.0 g) and $H_3PO_4$ (26.0 g), to which graphite powder (0.1 g) was added, followed by stirring for 1 min. Then the mixture was immediately covered and relocated into an ultrasonic bath (200 W and 42 kHz) for a special 60 min treatment consisting of simultaneous oxidization and ultrasonication. A cooler was connected to the bath to prevent heat buildup. During the treatment, graphite flakes may exfoliate and split into graphene sheets; meanwhile, they were oxidized by $Mn_2O_7$, which was created by $2KMnO_4(s) + H_2SO_4(aq) \rightarrow Mn_2O_7(l) + K_2SO_4 + H_2O$. The reaction can be terminated at anytime by moving the mixture out of the bath and then slowly adding 120 g of water, followed by vacuum filtration and washing three times with water and hydrogen peroxide for removal of ions and acids.

Graphene sheets of a medium degree of oxidation (medium-oxidation graphene) were made by dissolving $KMnO_4$ (0.4 g) in $H_2SO_4$ (26.0 g) and $H_3PO_4$ (26.0 g); high-oxidation graphene sheets were made by dissolving $KMnO_4$ (0.4 g) in $H_2SO_4$ (26.0 g) and $H_3PO_4$ (13.0 g). This is followed by a process similar to the fabrication of low-oxidation graphene. The treatment was terminated by relocating the beaker into an ice bath to prohibit rapid temperature rise and then slowly adding 120 g of water into the beaker, followed by a similar washing process. The prepared sheets were stored in solvents such as water or acetone for the following membrane fabrication. For characterization of powder samples, the sheets were dried in an air-ventilated oven at 60 °C and then in a vacuum oven at 100 °C for 4 h to remove crystalline water.

**2.3. Fabrication of Graphene Membranes.** The as-prepared sheets were suspended in water by 10 min of sonication. Then the suspension (0.64 mg/mL in water) was carefully filtered through a polypropylene filter membrane (47 mm diameter and 0.5 $\mu$m pore size) by a vacuum. The resultant graphene membranes were then dried at ∼60 °C overnight to remove water residue.


DOI: 10.1021/am5091287
ACS Appl. Mater. Interfaces 2015, 7, 13745−13757

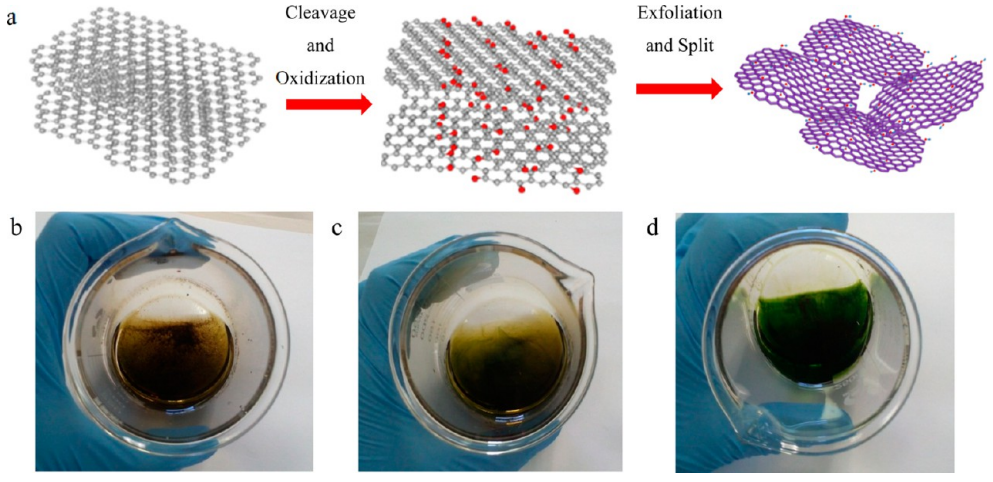


**Figure 2.** Schematic for the fabrication of graphene sheets (a). $KMnO_4$ prior to ultrasonication dissolved in mixtures of $H_3PO_4/H_2SO_4$ having ratios of (b) 1:2, (c) 1:1, and (d) 2:1.

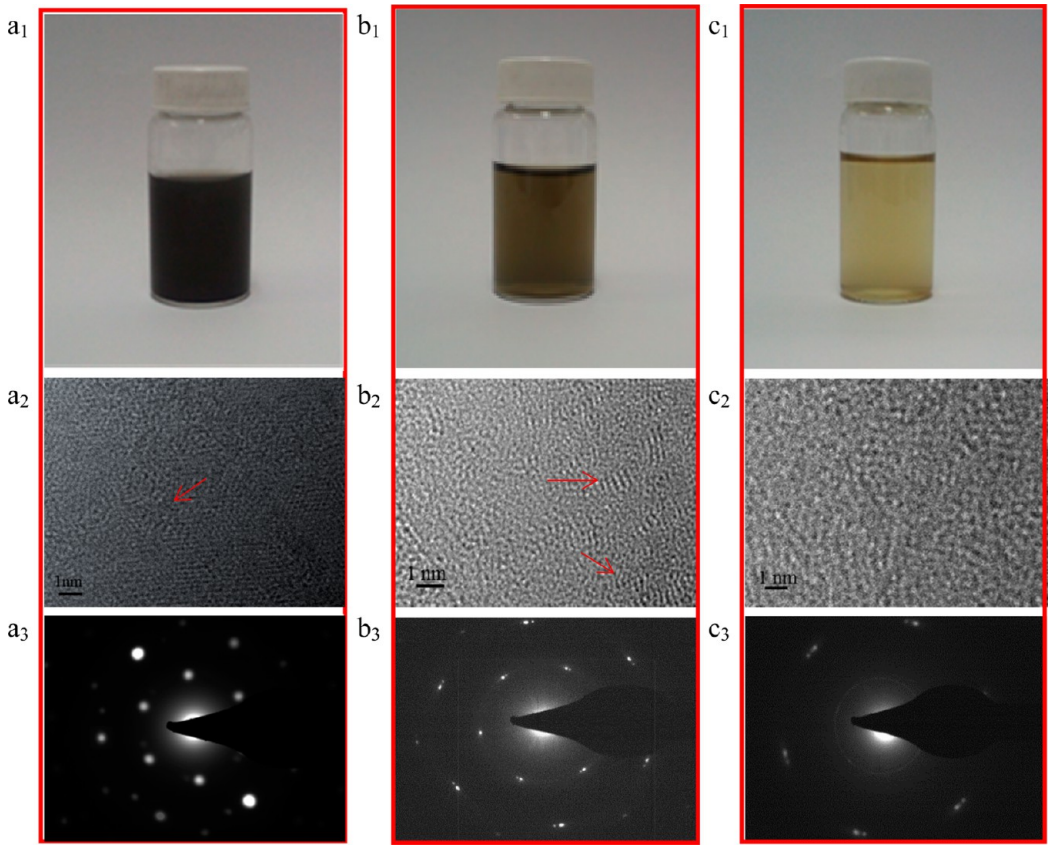


**Figure 3.** Graphene suspensions (1 mg/mL) after 1 week of storage, their TEM micrographs, and related diffraction patterns: (a) low oxidation; (b) medium oxidation; (c) high oxidation.

**2.4. Characterization.** X-ray diffraction (XRD) measurements were performed using a diffraction technology mini-materials analyzer. The diffractometer was equipped with curved graphite monochromators, tuned to Cu K$\alpha$ radiation ($\lambda$ = 1.5419 Å) with a tube voltage applied at 35 kV and 28.2 mA (1 kW). The diffraction patterns were collected in a reflection-mode geometry between $2\theta$ = 2 and 50° at a scan rate of 1°/min.

Atomic force microscopy (AFM) micrographs were obtained by using a NT-MDT NTEGRA SPM instrument with NSG03 noncontact "golden" cantilevers. The magnitude of oscillation was 15 nm, and the scan rate for 2 × 2 $\mu$m images was typically 0.5 Hz. The samples were prepared by suspending the sheets in *N*-methyl-2-pyrrolidone at 0.0004 wt % by 30 min of ultrasonication below 30 °C and then dropping the suspension on a silicon wafer followed by drying. A 100 $\mu$m scanner was used, with calibration done by 1.5 $\mu$m grids with a height of 22 nm.

Raman spectra were recorded at room temperature by a Renishaw in Via Raman microspectrometer with 633 nm laser excitation and notch filter cutting at ~100 $cm^{-1}$. Extreme care was taken to avoid sample damage or laser-induced heating. Measurements were performed from 4.00 to 0.04 mW incident power.

The functional groups of graphene sheets were characterized using a PerkinElmer 65 Fourier transform infrared (FTIR) spectrometer with a MIRacle single-reflection attenuated total reflectance accessory. X-


DOI: 10.1021/am5091287
ACS Appl. Mater. Interfaces 2015, 7, 13745−13757

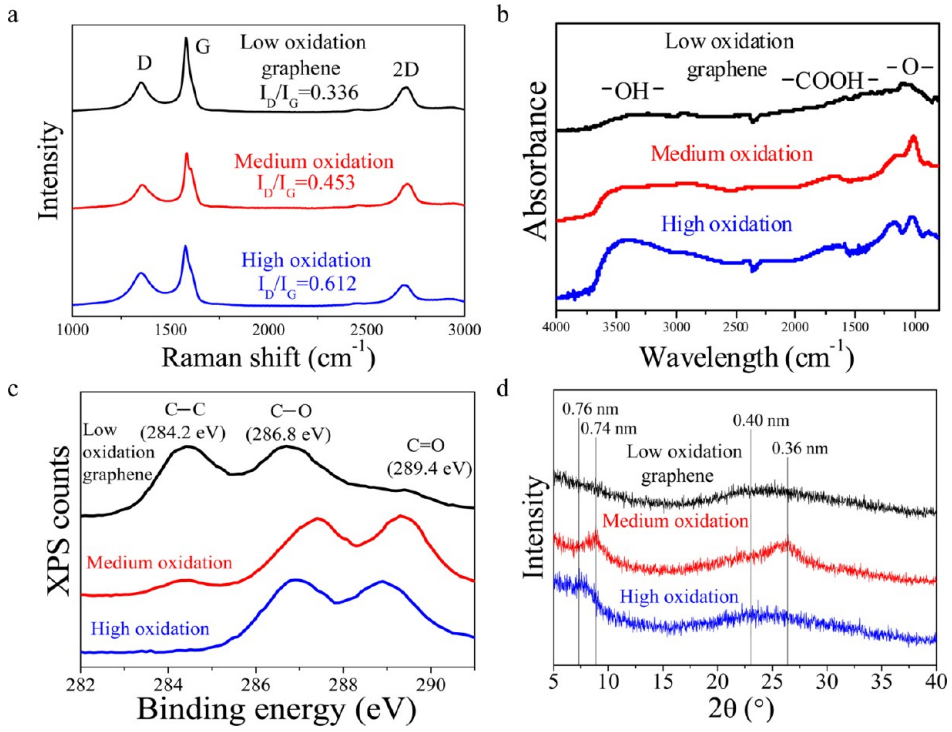


**Figure 4.** Identification of the chemical composition of graphene by (a) Raman, (b) FTIR, and (c) XPS spectra and (d) XRD patterns.

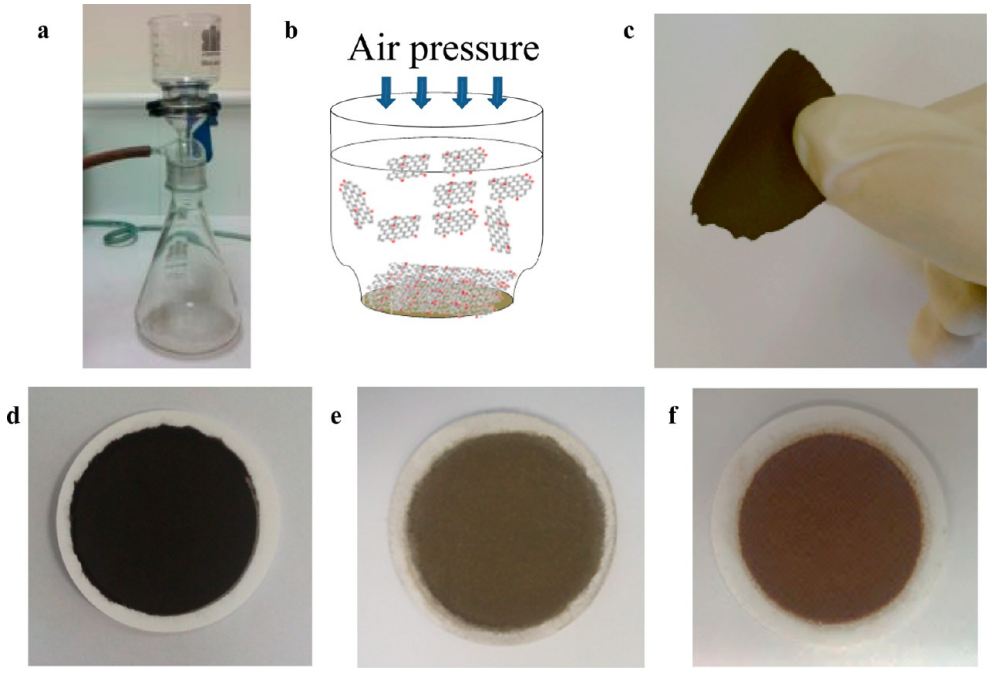


**Figure 5.** Schematic of vacuum filtration: (a) vacuum-filtration facility; (b) direct-flow filtration enabling graphene sheets horizontally aligned; (c) flexible yet mechanically robust medium-oxidation graphene membrane. Membranes coated on filtration paper with oxidation degrees of (d) low, (e) medium, and (f) high.

ray photoelectron spectroscopy (XPS) analysis was conducted by a SPECS SAGE XPS system with a Phoibos 150 analyzer and an MCD-9 detector, which used nonmonochromated Mg K$\alpha$ radiation at 10 kV and 20 mA (200 W). The spot size analyzed was circular with a diameter of 3 mm.

Micrographs of transmission electron microscopy (TEM) were obtained with a Philips CM200 at an accelerating voltage of 200 kV. The samples were prepared by suspending graphene sheets in tetrahydrofuran at 0.0004 wt % by 0.5 h of sonication and then dropping the solution on 200-mesh copper grids, followed by drying. The bright-field high-magnification TEM images were taken from a JEOL 2100F microscope operated at 120 kV.

A data-physics contact-angle measurement system (OCA15) was employed to examine the wetting behavior of graphene membranes at room temperature. A contact angle was obtained by averaging five measurements at different locations of the same sample. In a typical measurement, a membrane was fixed on a substrate horizontally and


DOI: 10.1021/am5091287
ACS Appl. Mater. Interfaces 2015, 7, 13745−13757

then carefully immersed into a chamber with water. All data were calculated by *OCA* software.

The pure water flux ratios were performed on a filtration device driven by pressurized air. The area for water permeation in this device is ~3.14 $cm^2$. The membranes were fixed on a metal grid. The applied air pressure could be adjusted at 0−3 bar. Once the flux stabilized, a water flux value was obtained by measuring the mass of water collected every 2 min under a constant pressure.

The tensile testing samples were cut with a pair of scissors into rectangular strips of 45 × 10 × 0.02 mm. Tensile testing was performed at 0.5 mm/min (strain rate) at room temperature using an Instron 5567. Young's moduli were calculated using 0.005−0.6% strain. The measured graphene membranes have thicknesses of 10−20 $\mu$m for medium- and high-oxidized graphene membranes and ~100 $\mu$m for low-oxidized graphene because the 20-$\mu$m-thick membrane of low-oxidation graphene was found to be brittle.

**2.5. Electrochemical Characterization.** Electrochemical measurement was performed on a CHI660E workstation with a 6 M KOH aqueous electrolyte in a two-electrode configuration. Each membrane was cut into 1 × 1 $cm^2$ and used as electrodes. Two pieces of platinum foil were used as the current collectors. The mass loading of the electrode material was about 1 mg/$cm^2$. The membranes were immersed in the electrolyte for 24 h before measurement. The capacitive performance was characterized by cyclic voltammetry (CV) and galvanostatic charge−discharge (GCD) techniques. The specific gravimetric capacitance of each electrode, $C$ (in F/g), was obtained from the discharge curve according to the following equation: $C = 4I\Delta t/m\Delta V$, where $I$ is the current load (A), $\Delta t$ is the discharge time (s), $\Delta V$ is the potential change during discharge (V), and $m$ is the mass loading on the total working electrode (g).

## 3. RESULTS AND DISCUSSION

**3.1. Synthesis of Graphene with Three Degrees of Oxidation.** By random selection of 50 graphene sheets that have a high degree of oxidation (high-oxidation graphene), the thickness was measured as 1.4 ± 0.5 nm; parts a and b of Figure 1 contain representative images. At low magnification, parts c and d of Figure 1, these sheets demonstrate a relatively uniform lateral dimension of 50−200 nm. By contrast, the starting material graphite is as thick as 70 nm (Figure 1e). The oxidation may first attack graphite edges, creating hydrophilic groups that thus increase the electrostatic repulsion between graphene layers,[27] leading to more efficient cleavage. The functional groups would help ultrasonication to chop large graphene sheets into smaller ones (Figure 2a). The graphene sheets with a low degree of oxidation can suspend in water (1 mg/mL) for at least 2 weeks. The suspensions will be utilized to fabricate membranes at a later stage.

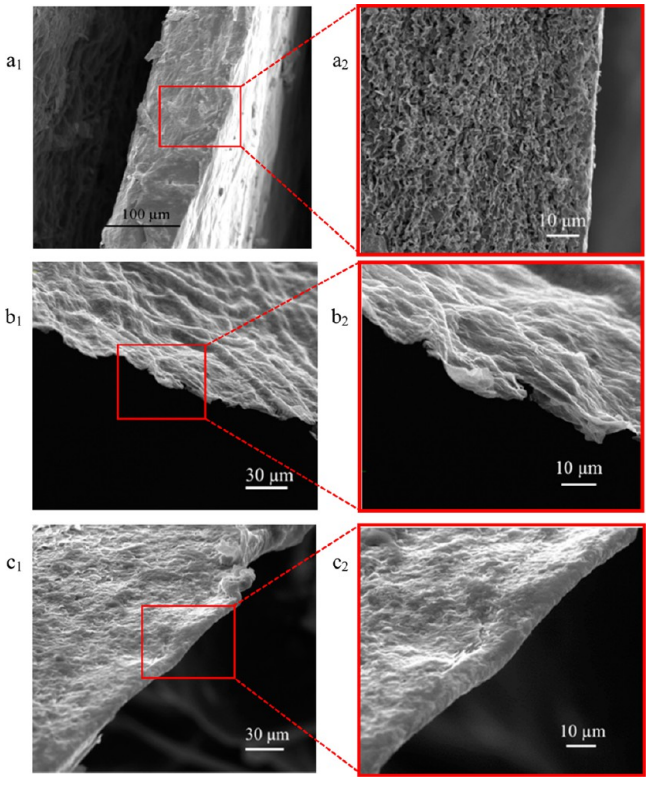


**Figure 6.** SEM micrographs of the edges of the graphene membranes with oxidation degrees of (a) low, (b) medium, and (c) high.

Figure 2 shows potential mechanisms for this 60 min process of graphene fabrication. The oxidation was made by $Mn_2O_7$ originating from the reaction between potassium permanganate and sulfuric acid: $2KMnO_4(s) + H_2SO_4(aq) \rightarrow Mn_2O_7(l) + K_2SO_4 + H_2O$. Dissolving $KMnO_4$ in $H_2SO_4$ produces $Mn_2O_7$, which is green in color, while dissolving $KMnO_4$ in $H_3PO_4$ produces $MnO_4^-$, which is purple in color. Because $Mn_2O_7$ has far more oxidation power than $MnO_4^-$, we can control the oxidation level by adjusting the ratio of $H_2SO_4$ to $H_3PO_4$ (Figure 2b−d); with an increase in the fraction, the solution color changed from (b) dark red for high-oxidation product to (d) yellow-green for low-oxidation graphene.

$H_3PO_4$ acted as a buffering agent to achieve a desired degree of oxidation. We also tried other acids including acrylic acid, formic acid, hydrogen chloride acid, and nitric acid, but only $H_3PO_4$ is the most suitable, as shown by the discussion in Figure S1 in the Supporting Information (SI).

The fraction of phosphoric acid plays a critical role in determining the oxidation degree of graphene (Figure $3a_1$−$c_1$) and thus its structural integrity and chemical composition. Parts $a_2$, $b_2$, and $c_2$ of Figure 3 illustrate high-resolution TEM micrographs of graphene sheets with three oxidation degrees. The low- and medium-oxidation sheets (Figure $3a_2$,$b_2$) consist of both crystalline regions characterized as ordered lattice and defective regions characterized as disordered clusters, as indicated by red arrows. The defective regions rich in hydrophilic oxygenated groups can improve dispersion in polar solvents such as water, while the crystalline regions corresponding to the integrity structure would provide excellent mechanical strength and electronic conductivity. With a decrease in the fraction of phosphoric acid, more functional groups were formed on the graphene surface to reach a relatively high oxidation level (Figure $3c_2$). The selected-area electron diffraction (SAED) patterns (Figure $3a_3$,$b_3$) exhibit typical 6-fold symmetry, consistent with the hexagonal crystalline structure of the graphene sheet. The changes of SAED in Figure $3c_3$ could be attributed to the increased amorphous functional groups. Notably, no vacancies can be found in our TEM observation, and this implies that even our high-oxidation graphene sheets have decent structural integrity. A large number of graphene sheets having similar lateral dimensions and thicknesses can be observed at low magnification in AFM micrographs (Figure S2 in the SI). The low lateral dimension would provide graphene sheets with more edges and thus higher electrostatic forces, preventing sheet stacking, which resulted in a longer suspending time.

Although Raman spectra were collected from the powder form, they are able to probe the evolution of the graphene structure during fabrication. In Figure 4a, all samples show peaks at around 1340, 1585, and 2690 $cm^{-1}$, which can be


DOI: 10.1021/am5091287
ACS Appl. Mater. Interfaces 2015, 7, 13745−13757

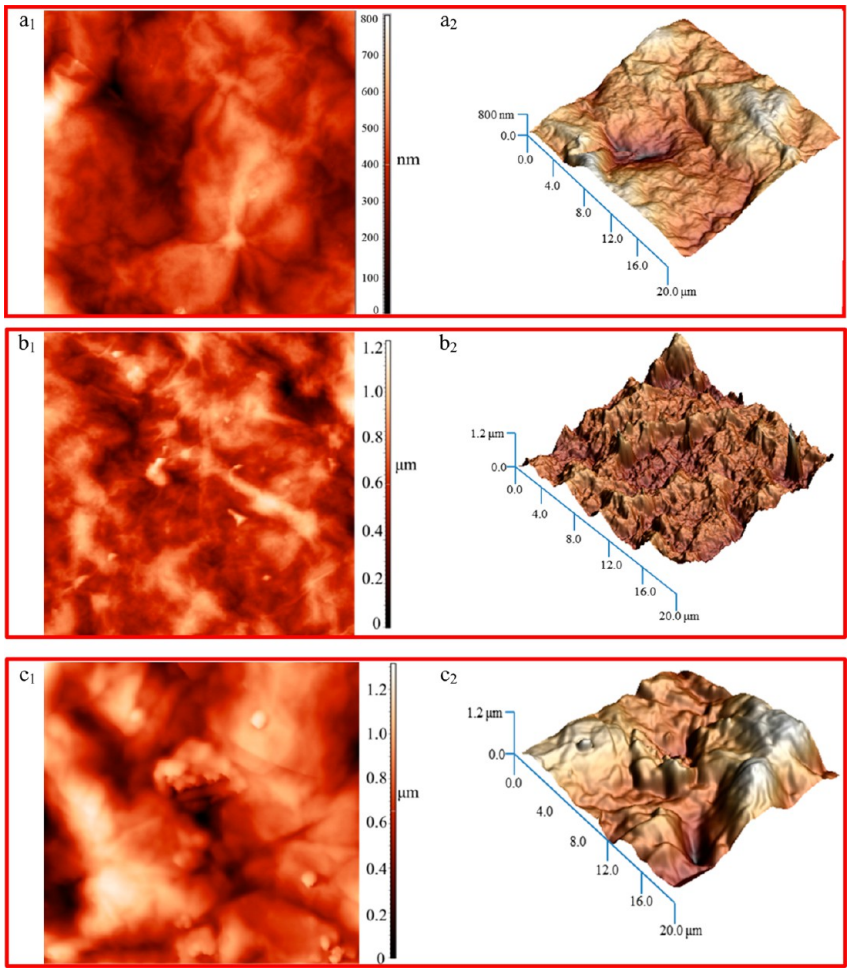


**Figure 7.** Tapping-mode AFM amplitude images (5 × 5 $\mu$m) and corresponding 3D surface plots of the membranes with oxidation degrees of (a) low, (b) medium, and (c) high.

respectively assigned to the D, G, and 2D peaks of carbon.[28] The G peak refers to a $sp^2$ resonance on an ordered graphitic lattice, and the D peak is activated from the first-order scattering process of $sp^2$ carbon atoms by the presence of substitutable in-plane heteroatoms, vacancies, grain boundaries, or other defects, which might be $sp^3$. The intensities of the G bands decrease with an increase in oxidation because $sp^2$-hybridized carbon atoms were evolved into $sp^3$-hybridized carbon atoms.[29]

The D/G intensity ratio increases from 0.336 (low-oxidation graphene) to 0.453 (medium-oxidation) to 0.712 (high) as the phosphoric acid fraction reduces. The ratios are proportional to the average size of the $sp^2$ domains.[30] In comparison with previous graphene sheets showing higher D/G ratios of 0.95−2,[31−33] our graphene sheets possess higher structural integrity. No observable difference can be seen between these 2D peaks, likely because all samples were tested in their powder form where most sheets stacked.

Because FTIR and XPS are often used to probe the chemical composition of inorganic materials,[34] these are employed herein. The FTIR spectra (Figure 4b) show the presence of hydroxyl groups (3400 $cm^{-1}$), carboxyl groups (1650 $cm^{-1}$), ether groups (1250 $cm^{-1}$), and C═C from nonoxidized $2p^2$ C−C bonds (1600 $cm^{-1}$). As the phosphoric acid fraction decreases, the absorption intensities at 3400, 1650, and 1250 $cm^{-1}$ increase, implying more oxygen-containing groups formed; this is also evidenced by XPS elemental analysis, where the C/O ratio decreases from 4.12 for low-oxidation graphene to 1.34 for the high-oxidation product (Figure S3 in the SI). The C/O atomic ratio was determined from the C 1s (~286 eV) core-level spectra (Figure S3 in the SI). In Figure 4c, the fitted peaks occurring at about 284.2, 286.2 and 289.8 eV usually correspond to the unoxidized $sp^2$ C═C bonds, hydroxyl or epoxide groups (C−OH or C−O−C), and carboxyl groups (C═O), respectively. The evolution of FTIR and XPS spectra indicates that the surface functionality of our graphene sheets can be readily controlled by adjusting the phosphoric acid fraction.

XRD (Figure 4d) analysis was performed to investigate the evolution of the graphene sheets. The patterns exhibit diffractions at ~26.5°, 22.6°, 8.76°, and 7.5° respectively corresponding to layer spacings of ~0.36, 0.4, 0.74, and 0.76 nm. With an increase in oxidation, the dominant graphitic layer spacing expands from 0.36 to 0.76 nm. In brief, increasing the oxidation level expands the graphene layer spacing.

**3.2. Graphene Membrane Structure.** Convenient processability and 2D molecular morphology of graphene sheets enable us to develop membranes by ordered assembling of sheets through vacuum-filtering of graphene suspensions (0.64 mg/mL; Figure 5a). Compression induced by a vacuum was responsible for aligning the graphene sheets perpendicular to the flow direction, and it narrowed the interspacing between


DOI: 10.1021/am5091287
ACS Appl. Mater. Interfaces 2015, 7, 13745−13757

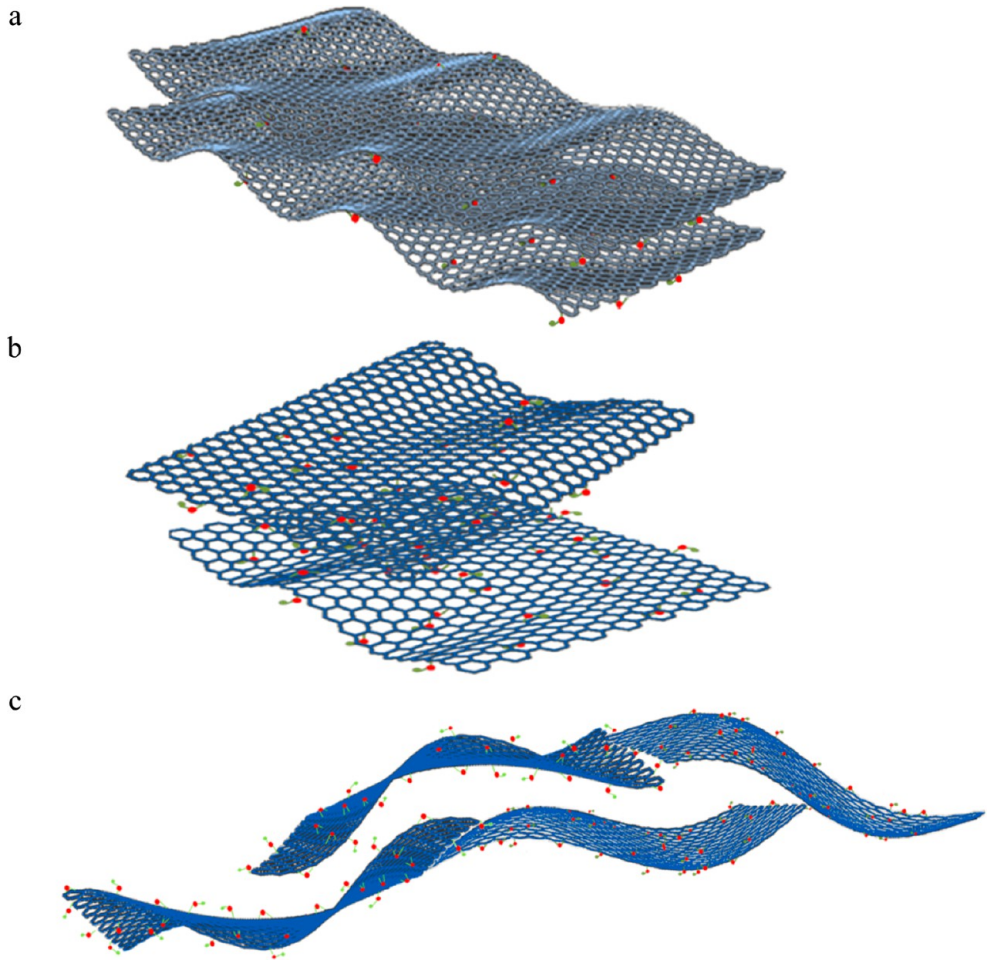


**Figure 8.** Schematics of the multilayered structure of graphene membranes with oxidation degrees of (a) low, (b) medium, and (c) high. The blue lines denote graphene sheets, and the red and green dots represent oxygen-containing functional groups.

the oriented graphene sheets; this promoted a higher degree of parallel arrangement of graphene sheets (Figure 5b). After filtration, graphene sheets were found to cover the filtration paper completely, forming a membrane where graphene sheets connected with each other side by side and stacked face by face. The prepared graphene membrane is flexible yet mechanically robust (Figure 5c) because of interaction of the van der Waals forces and hydrogen bonding between graphene sheets. Parts d−f in Figure 5 contain images of graphene membranes of three levels of oxidation. The membranes of 10−20 $\mu$m thickness were made through 2−4 h of simple vacuum filtration; the thickness can be well controlled by the quantity of the aqueous graphene solution.

We selected a thickness of 10−20 $\mu$m for the fabrication of medium- and high-oxidation membranes; because the 20-$\mu$m-thick membrane of low-oxidation graphene was found to be brittle, we increased the thickness to 100 $\mu$m. Figure 6 contains SEM micrographs of the membrane edges; these images have no observable cracks; graphene sheets may connect with each other on both the edges and basal planes via the vacuum-induced directional flow. An observable porous structure is found at the edge of the low-oxidation membrane (Figure 6$a_2$). The specific areas of three oxidized graphene membranes were investigated by $N_2$ absorption/desorption isotherms, and the result is indicated in section 4 in the SI. An obvious corrugated multilayer structure is observed on the medium- and high-oxidation graphene membrane surfaces (Figure 6$b_2$,$c_2$); the graphene's functional groups and crystalline water may assist in the formation of a stable network of interlayer hydrogen bonds, resulting in a relatively smooth cross section.

AFM analysis (Figure 7) indicates the surface morphological evolution of these graphene membranes. It is clear that the high- and medium-level membranes have stronger root-mean-square roughness (~1.2 $\mu$m) than the low-level membrane (~0.8 $\mu$m). The increase in the roughness can be explained by the fact that (i) the stronger oxidation creates more functional groups, which could result in a slight fluctuation of the sheets (Figure S4 in the SI) and (ii) after vacuum filtration, these graphene sheets of fluctuated structure tightly stack with each other, generating a corrugated membrane surface (Figure 8).

We now identify the formation mechanisms of these membranes. Of the three types of graphene membranes, the low-oxidation membrane was formed mainly by stable face-to-face interaction of the sheets (Figure 8a) because the low-oxidation graphene sheets have the least quantity of functional groups such as −COOH and −OH; these groups cannot absorb sufficient water molecules and thus produce the least layer expansion, as explained in Figure 4d. The medium- and high-oxidation membranes have more functional groups and thus more layer expansion; these groups would form clusters, and so the interaction between the clusters of different sheets would bend and buckle the sheets through hydrogen bonding. During filtration, the sheets could interact with each other between the faces and edges, causing "peak and valley"


DOI: 10.1021/am5091287
ACS Appl. Mater. Interfaces 2015, 7, 13745−13757

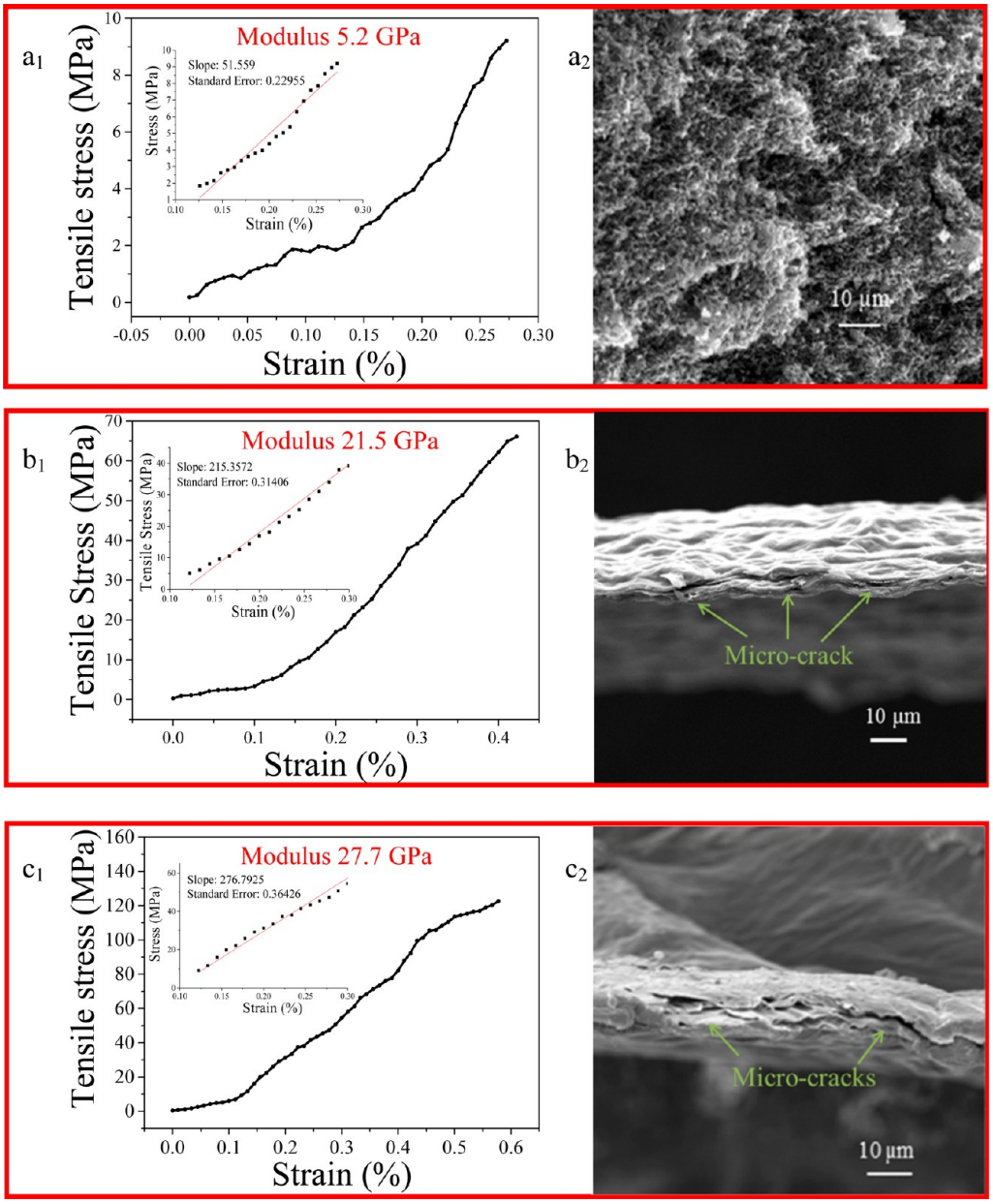


**Figure 9.** Typical stress−strain graphs and corresponding SEM images of the cross section of fractured membranes with oxidation degrees of (a) low, (b) medium, and (c) high.

undulation, resulting in fluctuated interlayer structure in medium and high graphene membranes schematically shown in Figure 8b. Because the edge-to-edge interactions were proven to be essential in determining the wrinkled structure,[35,36] "peaks" could be the most obvious at the combined interaction near the GO sheet edges during filtration, where the interacted sheets are buckled in the out-of-plane direction. After filtration, the stacking of functional group clusters between edges could become the "peaks", while the nonoxidized regions become the "valley".

**3.3. Mechanical Performance of Membranes.** The effect of oxidation on the mechanical performance of graphene membranes was examined through uniaxial tensile measurements with an Instron 2630-100 extensometer at room temperature. The stress−strain graphs are presented in Figure $9a_1$−$c_1$. The increase in oxidation enhances Young's modulus from 5.2 GPa for the graphene membrane of low oxidation degree (low-oxidation membrane) to 27.7 GPa for high-oxidation membrane; the tensile strength increases from 9.2 to 122.6 MPa. The increase in the tensile strength with oxidation corresponds to the fracture surface phenomenon in Figure $9a_2$−$c_2$, where the high-oxidation membrane shows the largest degree of deformation. The increment in the stiffness and strength can be explained in the wrinkling manner of graphene sheets, which could be formed by (i) the stretching, bending, and torsion of C−C bonds within the graphene sheets and (ii) the intersheet interactions, which mainly involve the relative displacement between GO sheets and the stretching of hydrogen bonds formed between the functional groups.[3]

The total potential energy of oxidized graphene membranes may consist of (i) the potential energy in each graphene sheet having wrinkles and (ii) the potential energy associated with intersheet interactions.[27] In the first stage of tensile deformation, stress increases steadily with strain, and this can


DOI: 10.1021/am5091287
ACS Appl. Mater. Interfaces 2015, 7, 13745−13757

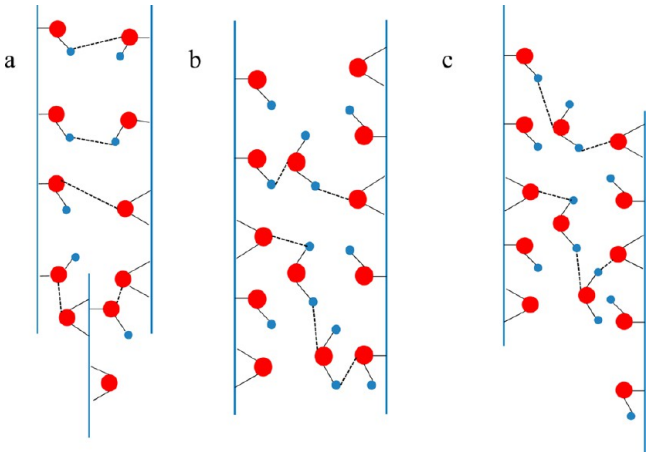


**Figure 10.** Schematic of (a) interlayer hydrogen bonding between functional groups in sheets, (b) interlayer hydrogen bonding formed between the functional groups of $H_2O$ and adjacent sheets, and (c) deformed interlayer hydrogen bonding under loading. Red and blue balls represent oxygen and hydrogen atoms, respectively, and black dashed lines represent hydrogen bonds formed.

be explained as the self-orientation of graphene sheets; the wrinkles of graphene sheets and the secondary bonds between graphene sheets would be stretched; as a result, the layered structures should be straightened and the sheets more aligned. In the second stage where the stress–strain graph shows a near-linear relationship with a higher slope, displacement between adjacent individual graphene sheets would occur. In this process, the out-of-plane edge–edge interaction could break because of the low potential energy and then form relatively stable face–face interaction.[3]

Hydrogen bonding plays a crucial role for intersheet interactions. Because of the presence of carboxyl, hydroxyl, and epoxy groups, graphene sheets are hydrated and would contain crystalline water. The hydrogen bonds formed immediately after sheet deposition can be subdivided into (i) the bonds between the intersheet water molecules and (ii) those between functional groups on each sheet.[35] Because of the lack of sufficient functional groups in the low-oxidation membrane, the reinforcement by hydrogen bonding is so insufficient that the membrane may break up just after the self-orientation step. The graphene membranes of medium and high levels of oxidation have sufficient functional groups and thus form extensive hydrogen-bonding networks, so both membranes are far stiffer and stronger. The high-oxidation membrane has the largest amount of functional groups and can produce the strongest hydrogen-bonding networks, leading to the highest stress value (Figure S5 in the SI).

The water molecules play a critical role in mediating the interactions between adjacent sheets, most likely via a hydrogen-bonding network formed between hydroxyl (both hydrogen-bond acceptor and donor) groups on the graphene surface. The content of water molecules of graphene membranes is investigated by thermogravimetric analysis measurements, as discussed in Figure S6 in the SI. Water molecules, which have rotational and translational degrees of freedom between the functional groups, would bridge the gap between adjacent sheets and increase the density of the hydrogen-bonding network. The hydroxide groups on the graphene sheets would likely form the majority of bridges (Figure 10a), but two or more water molecules could participate in the hydrogen-bonding network, where large gaps exist between adjacent sheets (Figure 10b). Because water molecules possess a certain degree of rotation, they can reorient themselves by breaking and making new hydrogen bonds with other sheets in response to external loading (Figure 10c). Under further loading, the interlamellar water molecules would reorient to activate fracture mechanisms such as slippage to dissipate energy, producing microcracks.[37]

When the stress reaches a sufficiently high level, breaking hydrogen bonding between the water molecules and oxygen-containing groups of graphene, water molecules are able to form new hydrogen bonds with other graphene sheets, so the sheets are able to accommodate some local sliding to relieve stress concentration.[38] Consequently, the high-oxidation membrane demonstrates the highest mechanical performance, such as Young's modulus of 27.7 GPa.

The uniaxial tension could lead to an equal distribution of stress across the samples, which is transferred mostly through the interlamellar shear deformation. The stress at the outer surface is transferred between the layers through the breaking and reforming of hydrogen bonds; further loading results in delamination of layers, particularly along the microcracks in the stacked structure. At the inner surface, this stress may be both compressive and shearing, which leads to local shearing and buckling of the layers.[39] So, the microcracks are expanded and propagated, as shown in Figure 11$a_2$–$c_2$. The interlayer adhesion and slippage of water molecules would lead to relatively slight slippage between adjacent sheets, causing interlamellar slippage (Figure 11$c_2$).

### 3.4. Water Permeation of Graphene Membranes.

Because graphene membranes showed sufficient mechanical strength, we proceeded to water permeation. Membranes of 10 $\mu$m thickness were placed onto a support grid that allowed us to apply an extra pressure of 3 bar. The flux rates were not recorded until steady state was reached. In Figure 12a, the flux rate increases nearly linearly with pressure for all of the membranes from 37.5 to 200.0 L/m$^2$·h·bar for the membrane with a low degree of oxidation (low-oxidation membrane) and from 15.0 to 120 and from 6.5 to 20 for the other two membranes; the low membrane shows the largest increment. Under the same pressure, the water flux reduces with an

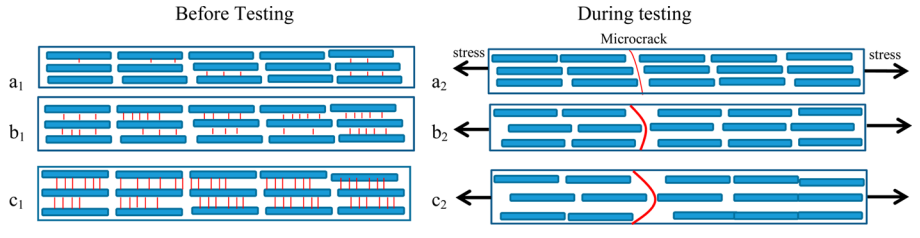


**Figure 11.** Schematics of tension-induced intersheet slippage of graphene membranes of different oxidation degrees: (a) low; (b) medium; (c) high.


DOI: 10.1021/am5091287
ACS Appl. Mater. Interfaces 2015, 7, 13745–13757

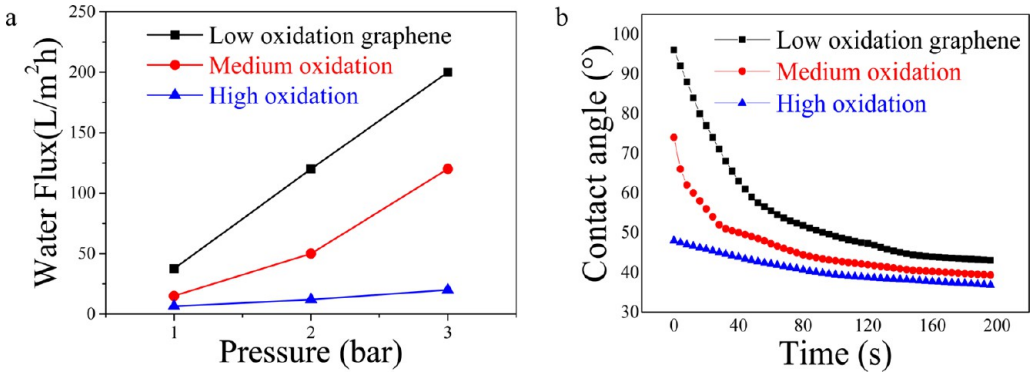


**Figure 12.** Membranes of three oxidation degrees (100 $\mu$m thickness made by coating ~70 mg of graphene sheets on polypropylene filtration paper): (a) water flux versus pressure; (b) evolution of the contact angle.

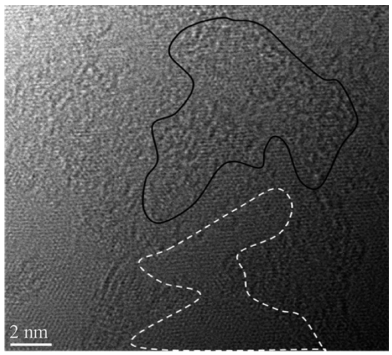


**Figure 13.** High-resolution TEM micrograph of a graphene sheet with a medium oxidation degree. The crystalline region, as circled by a white dashed line, would become the main open path for water transport, while the defective region, as circled by a black line, would impede water transport.

increase in the oxidation (Figure 12a). For example, at 1 bar of pressure, the flux decreases from 20 L/m$^2$·h·bar (low membrane) to 6.5 L/m$^2$·h·bar (high membrane). The flux values of medium and low graphene membranes are higher than those of Hummer's oxidized membranes (~3 L/m$^2$·h·bar) and similar to those of the reduced membranes (~20 L/m$^2$·h·bar).[40,41] The low-oxidation membrane demonstrates the highest flux value owing to its highest ratio of crystalline regions, which ensures a fast water permeation process; it is known that the oxidized regions absorb water molecules through hydrogen bonding.[42,43] Because of the higher proportion of oxidized regions, medium- and high-oxidation graphene membranes possess lower water flux values.

Through wettability measurement (Figure 12b), we investigated the effect of oxidization on the membrane roughness and water permeation rate. The membranes of three oxidation degrees show contact angles at 48°, 75°, and 97°, inversely related to oxidization. The contact angles are determined by the ratio of oxidized regions to graphene regions. The oxidized regions rich in functional groups can produce hydrogen bonding, resulting in a lower water contact angle, while the graphene regions, prevailing in C−C and C═C bonds, can disrupt the dynamic hydrogen bonding and the dramatic migration of water molecules on the membrane surface, resulting in a higher water contact angle. In addition, the hierarchical structures caused by oxidation on the membrane surface could intensify the hydrophilicity.[44] The contact angle decreases with an increase in the observation time. It is explained by the fact that the water droplets slowly permeated through the graphene membranes' hierarchical structure, which could provide increasingly more diffusion pathways for water molecules.

The advantageously high water permeation rates of our membranes over the previous graphene membranes mainly depend on (i) the moderate oxidization condition (amorphous and crystalline regions clearly shown in Figure 13), resulting in lower hydrophilicity, (ii) the graphene corrugation forming channels for permeation, and (iii) the paths provided by interlayer space through filtration (Figure 14).[43] It is worth pointing out that water transport is actually facilitated by the unique paths formed by the boundaries of graphene sheets having a low lateral dimension of ~100 nm (Figure 1).

**3.5. Capacitance of Graphene Membranes as Supercapacitor Electrodes.** The mechanical robustness and the distinctively layered structure of our graphene membranes imply that they have the potential to be used as electrodes for supercapacitors. The electrode material size is 1 × 1 cm$^2$ with a density of ~0.4 g/cm$^3$. All electrochemical measurements used 6 M KOH as the electrolyte with a two-electrode configuration, which can measure the cell performance more accurately. The CV curve shows a near-rectangular shape for the membranes

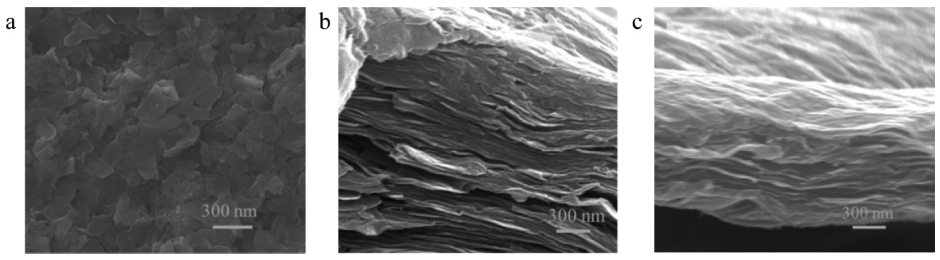


**Figure 14.** SEM images of graphene membranes with oxidation degrees of (a) low, (b) medium, and (c) high.


DOI: 10.1021/am5091287
ACS Appl. Mater. Interfaces 2015, 7, 13745−13757

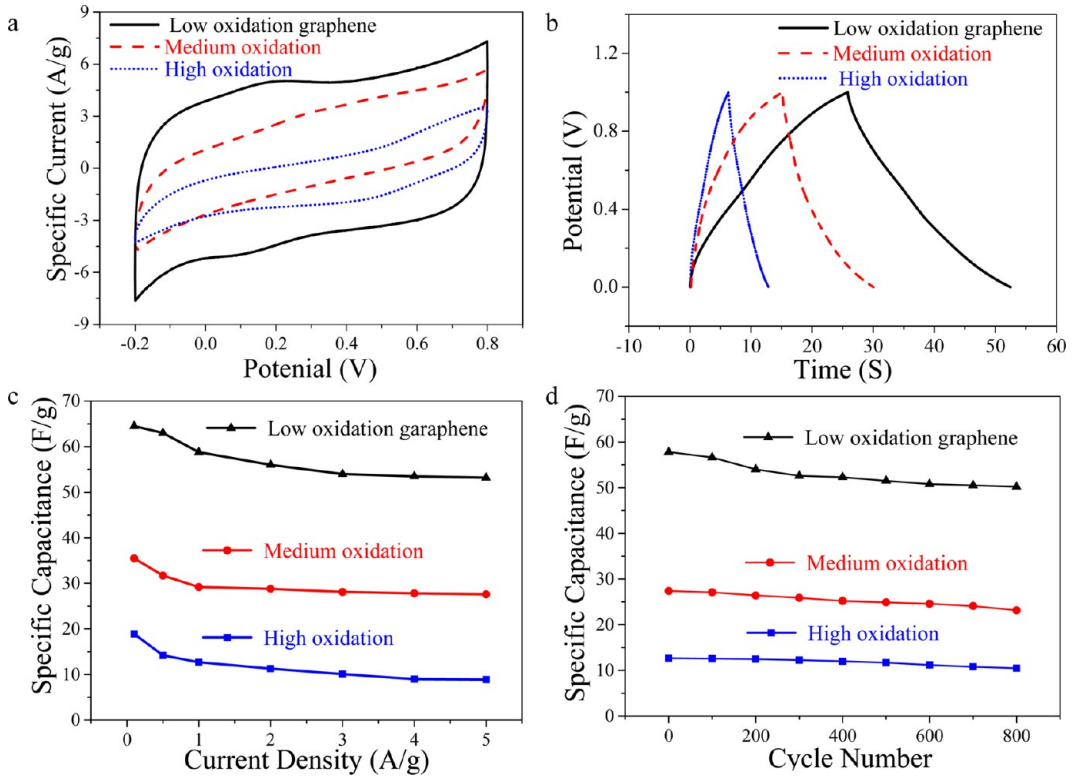


**Figure 15.** Electrochemical performance of graphene membranes with three oxidation levels using an aqueous electrolyte with two-electrode configuration: (a) CV curves at 0.1 V/s; (b) GCD curves at 1 V/s. Plots of specific capacitance versus (c) current density and (d) cycle number.

with low and medium oxidation, implying an electrochemical double-layer capacitance (EDLC) behavior (Figure 15a). EDLC can be attributed to the unique structure of the membranes (Figure 14), where interconnected channels made by filtration can provide a great many sites to trap ions and to transport electrolyte. The CV curve of the low-oxidation membrane shows one pair of slight Faradaic peaks, indicating pseudocapacitance, which may originate from the ion-exchange reactions at carbonyl groups: $C{=}O + e^- \leftrightarrow C{-}O^-$.

There are a number of factors determining the capacitance of electrode materials: (i) higher conductivity improves not only the power density but also the capacitance; (ii) functional groups, such as carbonyl, carboxyl, and hydroxide groups, contribute to the pseudocapacitance; (iii) interconnected, porous channels contribute to both high surface area for EDLC and redox reactions and a high flow rate of electrolyte; (iv) moderate wettability is desired because the aqueous electrolyte flow may be impeded by strong wettability.[45]

Of the graphene membranes with three degrees of oxidation, the high-oxidation membrane has the largest quantity of oxygen-containing groups contributing to the pseudocapacitance, so the highest capacitance was expected. Surprisingly, the low-oxidation membrane demonstrates the best performance, although it has the least quantity of oxygen-containing groups and pores. There might be two reasons for this. (i) The oxygen-containing groups of the high-oxidation membrane firmly lock water molecules, as shown by the lowest water flux in Figure 12a. This may impede the flow of the hydrophilic electrolyte through the membrane. Featuring the highest water flux rate (Figure 12a), the low-oxidation membrane should provide the best flow rate. (ii) The low-oxidation membrane has the highest electrical conductivity.

Figure 15b demonstrates GCD curves of the membranes tested at 1 A/g. With an increase in the oxidation, these membranes show specific capacitance at 58.8, 29.6, and 13.2 F/g and volume capacitance at 23.5, 11.8, and 5.3 F/cm$^3$. At a higher current density of 5 A/g, these gravimetric capacitance values respectively reduce to 53.2, 27.6, and 9.4 F/g and volumetric capacitance values reduce to 21.3, 11.1, and 3.8 F/cm$^3$ (Figure 15c). Because our vacuum filtration could form pores at nanoscale inside the membranes (Figure 14), the volume capacitance of the low-oxidation membrane is higher than the reported values of the low density film (~18 F/cm$^3$).[46] The charge/discharge measurements between −0.2 and 0.8 V at 1 A/g for 800 cycles show capacity retentions are 95.4%, 90.2%, and 86.7%, respectively, for the membranes (Figure 15d). This can be attributed to the high structural integrity of graphene and the mechanical robustness of the membranes. Our graphene membranes have the potential to be used as electrodes for various energy storage devices.

## 4. CONCLUSION

Graphene membranes with readily tunable degrees of oxidation were developed by vacuum-filtering of a graphene suspension. Through a special treatment consisting of simultaneous oxidization and ultrasonication, graphite particles were converted into graphene sheets of 1−3 nm thickness featuring high structural integrity (the Raman $I_D/I_G$ ratio increases from 0.34 to 0.71 with the oxidation degree). The water filtration rate and mechanical properties of graphene membranes can be readily controlled by tuning the oxidation level. Our synthesis method would promote the development of thin, high-flux, and efficient-sieving membranes because of their readily adjustable structures and properties. The membranes have potential


DOI: 10.1021/am5091287
ACS Appl. Mater. Interfaces 2015, 7, 13745−13757

applications as electrode materials for energy storage devices as well.

## ■ ASSOCIATED CONTENT

### Supporting Information

FTIR spectra, AFM micrographs of graphene sheets, graphene sheets with different oxidation degrees, C/O ratios, XPS analysis, TEM image of a wrinkled graphene sheet, specific surface areas, mechanical properties of graphene membranes, and water content. The Supporting Information is available free of charge on the ACS Publications website at DOI: 10.1021/am5091287.

## ■ AUTHOR INFORMATION


### Corresponding Author

*E-mail: Jun.Ma@unisa.edu.au.


### Author Contributions

The manuscript was written through contributions of all authors. All authors have given approval to the final version of the manuscript.

### Notes

The authors declare no competing financial interest.

## ■ ACKNOWLEDGMENTS

The authors are thankful for financial support by the Australian Research Council (Grant LP140100605). J.M. thanks Asbury for providing graphite.

## ■ REFERENCES


(1) Huang, H.; Ying, Y.; Peng, X. Graphene Oxide Nanosheet: an Emerging Star Material for Novel Separation Membranes. *J. Mater. Chem.* **2014**, *2*, 13772−13782.

(2) Lee, J. U.; Lee, W.; Yi, J. W.; Yoon, S. S.; Lee, S. B.; Jung, B. M.; Kim, B. S.; Byun, J. H. Preparation of Highly Stacked Graphene Papers via Site-selective Functionalization of Graphene Oxide. *J. Mater. Chem.* **2013**, *1*, 12893−12899.

(3) Lin, X.; Shen, X.; Zheng, Q.; Yousefi, N.; Ye, L.; Mai, Y. W.; Kim, J. K. Fabrication of Highly-aligned, Conductive, and Strong Graphene Papers using Ultralarge Graphene Oxide sheets. *ACS Nano* **2012**, *6*, 10708−10719.

(4) Brodie, B. C. On the Atomic Weight of Graphite. *Philos. Trans. R. Soc. London* **1859**, *149*, 249−259.

(5) Hummers, W. S.; Offeman, R. E. Preparation of Graphitic Oxide. *J. Am. Chem. Soc.* **1958**, *80*, 1339−1339.

(6) Marcano, D. C.; Kosynkin, D. V.; Berlin, J. M.; Sinitskii, A.; Sun, Z.; Slesarev, A.; Alemany, L. B.; Lu, W.; Tour, J. M. Improved Synthesis of Graphene Oxide. *ACS Nano* **2010**, *4*, 4806−4814.

(7) Park, S.; Lee, K. S.; Bozoklu, G.; Cai, W. W.; Nguyen, T. S.; Ruoff, R. S. G Graphene Oxide Papers Modified by Divalent Ions—Enhancing Mechanical Properties via Chemical Cross-Linking. *ACS Nano* **2008**, *2*, 572−578.

(8) Byon, H. R.; Lee, S. W.; Chen, S.; Hammond, P. T.; Horn, Y. S. Thin Films of Carbon Nanotubes and Chemically Reduced Graphenes for Electrochemical Micro-capacitors. *Carbon* **2010**, *49*, 457−467.

(9) Dichiara, A. B.; Sherwood, T. J.; Rogers, R. E. Binder Free Graphene-single-wall Carbon Nanotube Hybrid Papers for the Removal of Polyaromatic Compounds from Aqueous Systems. *J. Mater. Chem.* **2013**, *1*, 14480−14483.

(10) Becerril, H. A. B.; Mao, Jie.; Liu, Z.; Stoltenberg, R. M.; Bao, Z.; Chen, Y. E. Evaluation of Solution-Processed Reduced Graphene Oxide Films as Transparent Conductors. *ACS Nano* **2008**, *2*, 463−470.

(11) Huang, Z. D.; Zhang, B.; Oh, S. W.; Zheng, Q. B.; Lin, X. Y.; Yousefi, N.; Kim, J. K. Self-Assembled Reduced Graphene Oxide/Carbon Nanotube Thin Films as Electrodes for Supercapacitors. *J. Mater. Chem.* **2012**, *22*, 3591−3599.

(12) Sreeprasad, T. S.; Maliyekkal, S. M.; Pradeep, K. P. L. Reduced Graphene Oxide−metal/Metal Oxide Composites: Facile Synthesis and Application in Water Purification. *J. Hazard. Mater.* **2010**, *186*, 921−931.

(13) Verdejo, R.; Bernal, M. M.; Romasanta, L. J.; Lopez-Manchado, M. A. Graphene Filled Polymer Nanocomposites. *J. Mater. Chem.* **2011**, *21*, 3301−3310.

(14) Wang, L.; Lu, X.; Lei, S.; Song, Y. Graphene-based Polyaniline Nanocomposites: Preparation, Properties and Applications. *J. Mater. Chem.* **2014**, *2*, 4491−4509.

(15) Dichiara, A. B.; Sherwood, T. J.; Smith, J. B.; Wilson, J. C.; Weinstein, S. J.; Rogers, R. E. Free-standing Carbon Nanotube/graphene Hybrid Papers as Next Generation Adsorbents. *Nanoscale* **2014**, *6*, 6322−6327.

(16) Adhikari, B.; Biswas, A.; Banerjee, A. Graphene Oxide-Based Hydrogels to Make Metal Nanoparticle-Containing Reduced Graphene Oxide-Based Functional Hybrid Hydrogels. *ACS Appl. Mater. Interfaces* **2012**, *4*, 5472−5482.

(17) Tang, Z. H.; Wu, X. H.; Guo, B. C.; Zhang, L. Q. Preparation of Butadiene−styrene−vinylpyridine Rubber−graphene oxide Hybrids through Co-coagulation Process and in situ Interface Tailoring. *J. Mater. Chem.* **2012**, *22*, 7492−7501.

(18) Tang, L. C.; Wang, X.; Gong, L. X.; Peng, K.; Zhao, L.; Chen, Q.; Wu, L. B.; Jiang, J. X.; Lai, G. Q. Creep and Recovery of Polystyrene Composites Filled with Graphene Additives. *Compos. Sci. Technol.* **2014**, *91*, 63−70.

(19) Sumboja, A.; Foo, C. Y.; Wang, X.; Lee, P. S. Large Areal Mass, Flexible and Free-Standing Reduced Graphene Oxide/Manganese Dioxide Paper for Asymmetric Supercapacitor Device. *Adv. Mater.* **2013**, *25*, 2809−2915.

(20) Chua, C. K.; Pumera, M. Chemical Reduction of Graphene Oxide: a Synthetic Chemistry Viewpoint. *Chem. Soc. Rev.* **2014**, *43*, 291−312.

(21) Yang, X. M.; Tu, Y. F.; Li, L.; Shang, S. M.; Tao, X. M. Well-Dispersed Chitosan/Graphene Oxide Nanocomposites. *ACS Appl. Mater. Interfaces* **2010**, *2*, 1707−1713.

(22) Zeng, C. F.; Tang, Z. H.; Guo, B. H.; Zhang, L. Q. Supramolecular Ionic Liquid Based on Graphene Oxide. *Phys. Chem. Chem. Phys.* **2012**, *14*, 9838−9845.

(23) Shi, G.; Michelmore, A.; Jin, J.; Chen, Y.; Wang, L.; Yu, H.; Wallace, G.; Gambhir, S.; Zhu, S.; Talemi, H. P. Advancement in Liquid Exfoliation of Graphite through Simultaneously Oxidizing and Ultrasonicating. *J. Mater. Chem.* **2014**, *2*, 20382−20392.

(24) Wang, H.; Robinson, J. T.; Li, X.; Dai, H. Solvothermal Reduction of Chemically Exfoliated Graphene Sheets. *J. Am. Chem. Soc.* **2009**, *131*, 9910−9911.

(25) Guo, L. Z.; Wan, Y. J.; Yan, D.; Tang, L. C.; Wu, L. B.; Jiang, J. X.; Lai, G. Q. Toward Effective and Tunable Interphases in Graphene Oxide/Epoxy Composites by Grafting Different Chain Lengths of Polyetheramine onto Graphene Oxide. *J. Mater. Chem.* **2014**, *2*, 15058−15069.

(26) Chang, H.; Wang, G.; Yang, A.; Tao, X.; Liu, X.; Shen, Y.; Zheng, Z. A Transparent, Flexible, Low-Temperature, and Solution-Processible Graphene Composite Electrode. *Adv. Funct. Mater.* **2010**, *20*, 2893−2902.

(27) Gadipelli, S.; Calizo, I.; Ford, J.; Cheng, G.; Walker, A. R. H.; Yildirim, T. A Highly Practical Route for Large-area, Single Layer Graphene from Liquid Carbon Sources such as Benzene and Methanol. *J. Mater. Chem.* **2011**, *21*, 16057−16065.

(28) Shen, X.; Lin, X.; Yousefi; Jia, J. J.; Kim, J. K. Wrinkling in Graphene Sheets and Graphene Oxide Papers. *Carbon* **2014**, *66*, 84−92.

(29) Medhekar, N. V.; Ramasubramaniam, A.; Ruoff, R. S.; Shenoy, V. B. Hydrogen Bond Networks in Graphene Oxide Composite Paper: Structure and Mechanical Properties. *ACS Nano* **2010**, *4*, 2300−2306.

(30) Gao, Y.; Liu, L. Q.; Zu, S. Z.; Peng, K.; Zhou, D.; Han, B. H.; Zhang, Z. The Effect of Interlayer Adhesion on the Mechanical




DOI: 10.1021/am5091287
*ACS Appl. Mater. Interfaces* 2015, 7, 13745−13757

Behaviors of Macroscopic Graphene Oxide Papers. *ACS Nano* **2011**, *5*, 2134−2141.
(31) Putz, K. W.; Compton, O. C.; Palmeri, M. J.; Nguyen, S. T.; Brinson, L. C. High-Nanofiller-Content Graphene Oxide−Polymer Nanocomposites via Vacuum-Assisted Self-Assembly. *Adv. Funct. Mater.* **2010**, *20*, 3322−3329.
(32) Dikin, D. A.; Stankovich, S.; Zimney, E. J.; Piner, R. D.; Dommett, G. H. B.; Evmenenko, G.; Nguyen, S. T.; Ruoff, R. S. Preparation and Characterization of Graphene Oxide Paper. *Nature* **2007**, *448*, 457−460.
(33) Han, Y.; Xu, Z.; Gao, C. Ultrathin Graphene Nanofiltration Membrane for Water Purification. *Adv. Funct. Mater.* **2013**, *23*, 3693−3700.
(34) Ma, J.; Feng, Q. Y.; Shi, L. H.; Xu, J. Preliminary Study on Pyrolysis of Polymethylsilsesquioxane by FT-IR and XPS. *Chin. Chem. Lett.* **2002**, *13*, 75−78.
(35) Nicolaï, A.; Sumpter, B. G.; Meunier, V. Tunable Water Desalination across Graphene Oxide Framework Membranes. *Phys. Chem. Chem. Phys.* **2014**, *16*, 8646−8654.
(36) Tang, L. A. L.; Lee, W. C.; Shi, H.; Wong, E. Y. L.; Sadovoy, A.; Gorelik, S.; Hobley, J.; Lim, C. T.; Loh, K. P. Highly Wrinkled Cross-Linked Graphene Oxide Membranes for Biological and Charge-Storage Applications. *Small* **2012**, *8*, 423−431.
(37) Wei, N.; Peng, X.; Xu, Z. Understanding Water Permeation in Graphene Oxide Membranes. *ACS Appl. Mater. Interfaces* **2014**, *6*, 5877−5883.
(38) Chen, Z.; Dong, L.; Yang, D.; Lu, H. Superhydrophobic Graphene-Based Materials: Surface Construction and Functional Applications. *Adv. Mater.* **2013**, *25*, 5352−5359.
(39) Han, S.; Wu, D.; Li, S.; Zhang, F.; Feng, X. Porous Graphene Materials for Advanced Electrochemical Energy Storage and Conversion Devices. *Adv. Mater.* **2014**, *26*, 849−864.
(40) Yang, X.; Cheng, C.; Wang, Y.; Qiu, L.; Li, D. Liquid-Mediated Dense Integration of Graphene Materials for Compact Capacitive Energy Storage. *Science* **2013**, *341*, 534−537.
(41) Nicolaï, A.; Sumpter, B. G.; Meunier, V. Tunable Water Desalination across Graphene Oxide Framework Membranes. *Phys. Chem. Chem. Phys.* **2014**, *16*, 8646−8654.
(42) Tang, L. A. L.; Lee, W. C.; Shi, H.; Wong, E. Y. L.; Sadovoy, A.; Gorelik, S.; Hobley, J.; Lim, C. T.; Loh, K. P. Highly Wrinkled Cross-Linked Graphene Oxide Membranes for Biological and Charge-Storage Applications. *Small* **2012**, *8*, 423−431.
(43) Wei, N.; Peng, X.; Xu, Z. Understanding Water Permeation in Graphene Oxide Membranes. *ACS Appl. Mater. Interfaces* **2014**, *6*, 5877−5883.
(44) Chen, Z.; Dong, L.; Yang, D.; Lu, H. Superhydrophobic Graphene-Based Materials: Surface Construction and Functional Applications. *Adv. Mater.* **2013**, *25*, 5352−5359.
(45) Han, S.; Wu, D.; Li, S.; Zhang, F.; Feng, X. Porous Graphene Materials for Advanced Electrochemical Energy Storage and Conversion Devices. *Adv. Mater.* **2014**, *26*, 849−864.
(46) Yang, X.; Cheng, C.; Wang, Y.; Qiu, L.; Li, D. Liquid-Mediated Dense Integration of Graphene Materials for Compact Capacitive Energy Storage. *Science* **2013**, *341*, 534−537.



DOI: 10.1021/am5091287
*ACS Appl. Mater. Interfaces* 2015, 7, 13745−13757